DOI: 10.19884/j.1672-5220.202502017

A CFRP Hydrogen Maser Bell Jar with Excellent Gas-Barrier Performance

GAO Jiandong[1,2], XIAO De[1,2], CHENG Lele[1,2], CHEN Zhigang[1,2], SHUAI Tao[3*], ZHANG Lisha[4*], YU Muhuo[1,2], SUN Zeyu[1,2*]

1. State Key Laboratory of Advanced Fiber Materials, College of Materials Science and Engineering, Donghua University, Shanghai 201620, China
2. Shanghai Key Laboratory of Lightweight Structural Composites, Shanghai Collaborative Innovation Center of High-Performance Fibers and Composites (Province-Ministry Joint), Donghua University, Shanghai 201620, China
3. Shanghai Astronomical Observatory, Chinese Academy of Sciences, Shanghai 200030, China
4. College of Environmental Science and Engineering, Donghua University, Shanghai 201620, China

Abstract: This study investigated the optimization of gas-barrier performance in carbon fiber reinforced polymer (CFRP) laminates for hydrogen maser bell jars (HMBJs). Through systematic analysis of the effects of key factors, including ply count, curing process, and overlap mode, on the gas-barrier performance of CFRP laminates, a CFRP HMBJ with excellent gas-barrier performance was successfully produced via CATIA software design and a molding process. Compared with an aluminum alloy HMBJ, the molded CFRP HMBJ achieved a 34.9% reduction in mass, with a helium leakage rate as low as 9.04×10^{-7} Pa·m^3/s, meeting the performance requirements for hydrogen maser applications. The study reveals that gas leakage in CFRP laminates primarily occurs through diffusion along the fiber/resin interface, which provides a theoretical foundation for the development of molded CFRP HMBJs with both leak-tightness and structural optimization. Featuring low cost, simple process, and excellent gas-barrier performance, the molded CFRP HMBJ offers a reasonable solution for satellite HMBJs.

Keywords: carbon fiber reinforced polymer (CFRP); molding process; gas-barrier performance; resin curing system; interlayer overlap

CLC number: TB332 **Document code**: A

Article ID: 1672-5220(2026)05-0060-11

0 Introduction

In the field of spaceborne time and frequency technology, a lightweight spaceborne hydrogen maser is a major focus of current research worldwide. The hydrogen maser bell jar (HMBJ) has traditionally been made of AA 7075, but this material has reached its limits for further mass reduction, necessitating the search for lighter alternatives. A key strategy in reducing the mass of the spaceborne HMBJ involves substituting traditional metal with materials that offer greater strength and stiffness. Since the physical system of the passive hydrogen maser accounts for about 65% of its total mass, reducing the mass of the physical system is critical. Therefore, current efforts are concentrated on key parts such as the microwave cavity, HMBJ, magnetic shielding system, and associated physical and vacuum systems[1-2].

Carbon fiber reinforced polymers (CFRPs) not only have significant advantages of lightweight and high strength but also have the characteristics of strong designability, low thermal conductivity, and excellent dimensional stability, especially when compared with currently prevalent metal structural materials. At present, CFRPs have been successfully used in various aerospace structural products at home and abroad, such as bearing cylinders, structural plates, optical platforms, high-precision trusses, earth observation camera barrels, and antenna reflectors.

Currently, thermosetting carbon fiber composites with carbon fiber as the reinforcement material and epoxy resin as the matrix material are the most popular in spacecraft structures. These materials boast significant advantages in mechanical properties and thermal stability[3]. However, the properties of composites vary depending on the molding process used. The molding process of composites allows for high dimensional accuracy, ensures internal molding quality, and is ideal for the integrated molding of complex composite structural components. Die pressing plays a crucial role in composite molding, as varying die pressing parameters can impact the uniformity of compression and resin flow in the mold cavity, significantly affecting the quality of the composite molding[4-6]. Excessive mold pressure can cause issues like buckling, fiber breakage, and interlayer

Received date: 2025-02-27

Foundation items: Open Research Funds of State Key Laboratory of Advanced Fiber Materials, China (No. KF2203); Fundamental Research Funds for the Central Universities, China (No. 2232024D-12)

* Correspondence should be addressed to SUN Zeyu, email: sunzeyu@dhu.edu.cn; SHUAI Tao, email: shuait@shao.ac.cn; ZHANG Lisha, email: lszhang@dhu.edu.cn

Citation: Gao J D, Xiao D, Cheng L L, et al. A CFRP hydrogen maser bell jar with excellent gas-barrier performance[J]. *Journal of Donghua University (English Edition)*, 2026, 43(5): 60-70.

cracking in the molding of composite structures, leading to performance failures. Therefore, it is necessary to optimize mold design through finite element analysis, which is an important method to improve the rationality of mold design[7-9]. The gas-barrier performance of composites should be considered in the application of spacecraft. The current understanding of the gas leakage mechanism in composites revolves around two theories: diffusion permeability and microcrack leakage, both influenced by the material composition, layout design, and molding process. Therefore, improving the gas-barrier performance of composites can be achieved by focusing on these two leakage mechanisms[10-13].

Current research on enhancing the gas-barrier performance of composite materials primarily revolves around refining their composition, optimizing their structural design, and enhancing the properties of matrix materials. In resin matrix composites, the presence of free volume within the resin matrix offers an opportunity to boost both leakage resistance and mechanical properties by incorporating nanoparticles[14]. The effectiveness of this approach lies in the nanoparticles filling the free volume within the resin matrix, altering the internal void distribution, and thereby extending the path for gas leakage, which reduces the overall leakage potential of the composite. Leakage mechanisms in composites indicate that internal microcracks are a primary contributor to the high leakage rates observed in these materials. Therefore, optimizing the layup configuration can enhance leakage resistance by improving the internal stress distribution and reducing stress concentrations that promote microcrack formation. Ultimately, suppressing microcrack initiation and propagation under external loads is key to achieving low leakage in fiber-reinforced composites[15-22].

Current research on leakage resistance has focused primarily on composite hybrid lamination techniques. Based on the microcrack theory, the gas leakage pathway can be significantly lengthened by incorporating single or multiple unbroken plies within the layered structure of the composite. Consequently, an essential approach to improving leakage resistance involves integrating metals and polymer film layers into composite materials. This strategy ensures that even if microcracks are present within the composites, the materials maintain effective leakage resistance[23-28].

This study aimed to develop a lightweight and high-performance HMBJ by exploring the material performance of CFRP HMBJ and enhancing its gas-barrier performance. A comprehensive forming system was established, encompassing material selection, structure design, process optimization, and performance evaluation. The gas-barrier performance of the CFRP HMBJ was analyzed, and three key process parameters were optimized. The HMBJ was fabricated via die pressing, and its axial compression capabilities and overall leakage rate were experimentally evaluated.

1 Experimental Section

1.1 Preparation of experimental materials and samples

The fabrication process of the molded CFRP HMBJ is illustrated in Fig. 1. Initially, three layers of plain weave prepreg (T300-3K, Weihai Baowei New Material Technology Co., Ltd., China) were laid up on the inner mold to form the outer shell. Pre-impregnated fiber rings were then circumferentially wrapped around steel reinforcement bars, with aluminum alloy reinforcements positioned by an outer mold. During lay-up, particular attention was paid to minimizing ply overlap and ensuring uniform alignment. Subsequently, a vacuum bag pressing method was employed for pre-compaction, facilitating intimate contact between prepreg layers through preliminary vacuum evacuation. Based on Darcy's law[29], the resin flow front velocity at 0.6 MPa was matched with the heating rate to ensure adequate impregnation without excessive resin loss. After optimizing other parameters such as residence time and temperature, the component was transferred to an autoclave for final curing. Details of the curing process and parameters are summarized in Fig. 1(b).

The mass of the prepared CFRP HMBJ was approximately (540 ± 5) g, representing a reduction of approximately 34.9% from that of the AA 7075 HMBJ (830 g), thus meeting the criterion of at least a 30% reduction in mass.

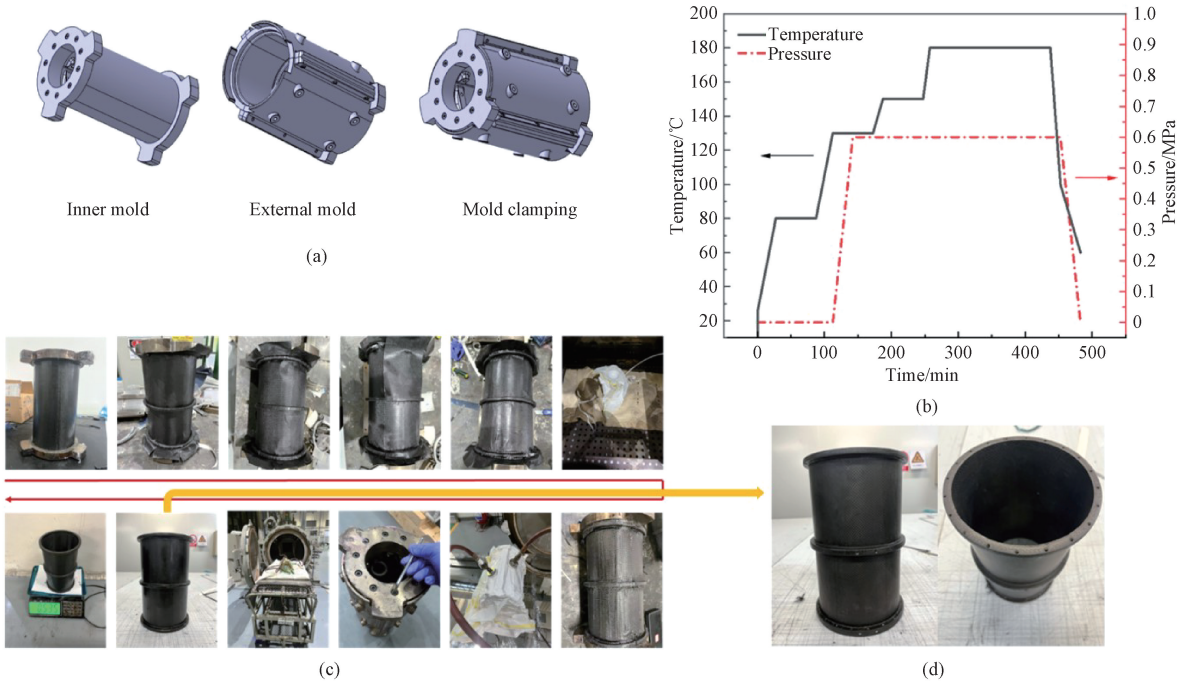


Fig. 1 Fabrication of CFRP HMBJ: (a) mold structure diagram; (b) process parameters; (c) CFRP HMBJ autoclave-assisted molding process; (d) CFRP HMBJ image

1.2 Characterization for CFRP laminates

The thermogravimetric analyzer (Netzsch, Germany) was used to measure the thermal stability and decomposition behavior of the cured CFRP laminates. The differential scanning calorimetry (DSC) instrument (Netzsch, Germany) was used to measure the curing reaction enthalpy change of the resin in composite materials. The non-isothermal DSC test was carried out under an inert N_2 atmosphere. The sample mass was 2–6 mg. The temperature range was 25 – 320 ℃ with heating rates of 5, 10, 15, and 20 ℃/min to investigate the curing behavior of the resin system. Subsequently, an isothermal DSC test was performed at 130, 150, and 180 ℃. Each sample was rapidly heated to the target temperature, and the heat flow was recorded until no further exothermic activity was detected, at which point the test was terminated to determine the cure time at each temperature.

The viscosity of the resin system was characterized using a high-temperature rotational rheometer (TA Instruments, USA). An appropriate sample was placed in the AA 6061 parallel plate fixture with a plate gap of 500 μm and an edge trimming gap of 50 μm. The rotational speed was set to 10 rad/s with a 3% strain applied. The experiment included non-isothermal and isothermal rheological tests. In non-isothermal rheological tests, the temperature increased at a rate of 3 ℃/min within the range of 25 to 200 ℃ to analyze the viscosity of the resin system as a function of temperature. In isothermal rheological tests, different constant temperatures (130, 140, 150, 160, and 180 ℃) were set. The sample was first rapidly heated to the specified constant temperature, and then maintained at that temperature for a period of time to analyze the viscosity of the resin system over time.

The morphology of the sample was observed by a scanning electron microscope (Hitachi, Japan). To minimize surface charging and improve conductivity, the sample was mounted on a stub with conductive adhesive and sputter-coated with gold for 3 min before observation.

1.3 Experimental design

The composite material of the HMBJ was a laminate consisting of multiple plies. This study investigated the effects of ply count, curing process, and overlap mode on the gas-barrier performance of CFRP laminates. Oxygen permeability and permeability coefficients of the CFRP laminates were measured under various processing conditions. Based on the analysis of the results, an optimized processing scheme was established to improve the gas-barrier performance. The experimental design for testing the gas-barrier performance of the CFRP laminate structure is detailed in Table 1.

Table 1 Experimental setup for testing gas-barrier performance of CFRP laminates

Sample	Ply count	Curing process	Overlap mode	Other conditions
S1	5	Medium-temperature	No lap	No grinding
S2	6	Medium-temperature	No lap	No grinding
S3	7	Medium-temperature	No lap	No grinding
S4	6	Low-temperature	No lap	No grinding
S5	6	High-temperature	No lap	No grinding
S6	6	Medium-temperature	No lap	With grinding
S7	6	Medium-temperature	Overlap 1	With grinding
S8	6	Medium-temperature	Overlap 2	With grinding
S9	6	Medium-temperature	Overlap 3	With grinding

Notes: Overlap 1, Overlap 2, and Overlap 3 denote three overlap modes, detailed in Subsection 2.3; the low-temperature, medium-temperature, and high-temperature curing processes were set as 115 ℃ (1 h)→130 ℃ (1 h) →150 ℃ (5 h), 130 ℃ (1 h) → 150 ℃ (1 h) →180 ℃ (3 h), and 150 ℃ (1 h) →180 ℃ (1 h) →200 ℃ (1 h), respectively.

1.4 Gas permeability test of CFRP laminates

The leakage test was conducted in accordance with GB/T 1038.1—2020. A GTR-721 gas transmission instrument (Fig. 2(a)) produced by Shandong Systester in China was used for testing. The schematic diagram of the test principle is shown in Fig. 2(b). Before the test, the test sample was placed between the upper and lower test chambers for overall vacuum extraction operation. The lower chamber was closed after the required vacuum degree was reached. The test gas was then filled into the upper chamber to form a 0.1 MPa pressure difference between the upper and lower chambers. Under this pressure difference, the test gas permeated from the high-pressure chamber (upper chamber) to the vacuum chamber (lower chamber). The gas transmission rate and gas permeability coefficient were calculated and converted into the leakage rate. Each sample was measured three times, and the average value was taken as the final result.

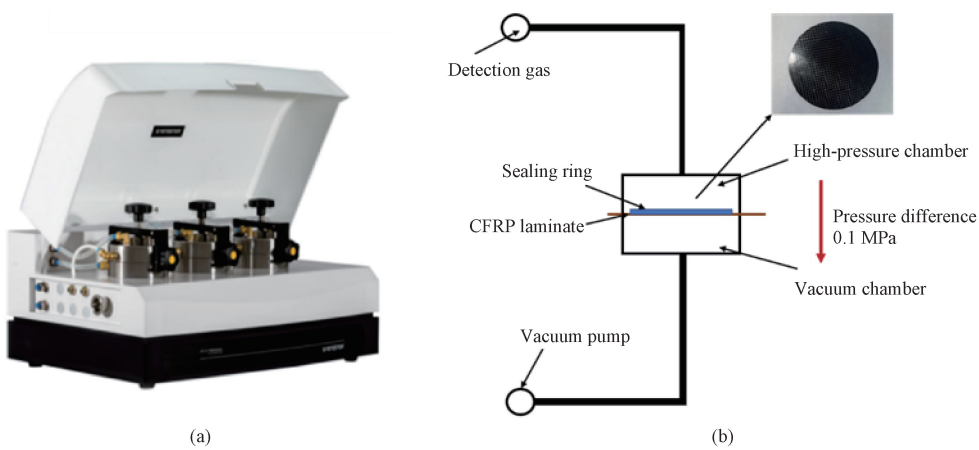


Fig. 2 Schematic of instrument and test principle of leakage test: (a) GTR-721 gas transmission instrument; (b) schematic diagram of test principle

1.5 Overall leakage rate test of HMBJ

The primary objective of sealing HMBJ is to prevent gases and impurities from degrading the accuracy and stability of the hydrogen maser. To validate the effectiveness of structural process optimization and enable performance comparisons with other specimens, the overall leakage rate of the HMBJ must be tested. A helium mass spectrometer leak detector, which is produced by INFICON in Switzerland, was employed to measure the total helium leakage rate, with real-time monitoring of helium content within the CFRP HMBJ.

2 Results and Discussion

2.1 Effect of ply count on gas-barrier performance

To investigate the gas leakage characteristics of CFRP laminates with varying ply counts and in line with the lightweight requirements of HMBJ, tests were conducted on the gas-barrier performance of CFRP laminates consisting of 5, 6, and 7 plies. The gas permeability curves of CFRP laminates with different ply counts are shown in Fig. 3, where the inset depicts the structure of the laminates.

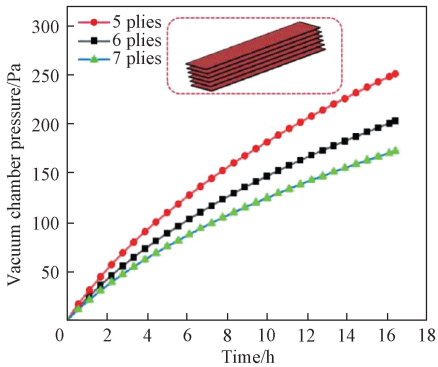


Fig. 3 Gas permeability curves of CFRP laminates with different ply counts

Figure 3 shows that as the ply count increases, the pressure within the vacuum chamber decreases correspondingly, indicating a gradual reduction in oxygen leakage rate (Table 2) and an improvement in gas-barrier performance. This enhancement is attributed to the longer and more intricate diffusion pathways for oxygen with increasing ply count. Considering both the lightweight requirement and the need to keep the leakage rate within acceptable limits, a six-ply structure was selected.

Table 2 Gas-barrier performance of CFRP laminates with different ply counts

Sample	Ply count	Oxygen transmission rate/ [$cm^3/(m^2 \cdot 24\ h \cdot Pa)$]	Oxygen permeability coefficient/ [$cm^3 \cdot cm/(cm^2 \cdot s \cdot Pa)$]	Oxygen leakage rate/ ($Pa \cdot m^3/s$)	Oxygen leakage rate deviation/ ($Pa \cdot m^3/s$)
S1	5	3.32×10^{-5}	3.99×10^{-15}	2.02×10^{-8}	0.075×10^{-8}
S2	6	3.06×10^{-5}	4.24×10^{-15}	1.86×10^{-8}	0.078×10^{-8}
S3	7	2.69×10^{-5}	4.34×10^{-15}	1.63×10^{-8}	0.067×10^{-8}

2.2 Effect of curing process on gas-barrier performance

For CFRP laminates, an appropriate curing process serves as the foundation for achieving superior gas-barrier performance. By regulating curing temperature and duration to ensure full resin infiltration into fibers, the interfacial bonding capability between the two phases is enhanced, forming a denser laminate structure. Therefore, based on a six-ply stacking configuration, this study evaluated and analyzed the gas-barrier performance of composites under three distinct curing processes (low-temperature curing, medium-temperature curing, and high-temperature curing), thereby exploring the influence of the curing process on the gas-barrier performance of composites. Before investigating the impact of the curing process on leakage rates, it was essential to establish the curing process for the epoxy resin system used in CFRP. Through characterization of the curing kinetics and rheological properties of the system, its curing process was determined. As shown in Fig. 4(a), the decomposition temperature of the resin system is 330 ℃, indicating optimal thermal stability. As shown in Fig. 4(b), the thermal decomposition rate of the resin system peaks at 408 ℃, with a cumulative mass loss of 48.63% (Fig. 4(a)) within the 320–480 ℃ range. The decomposition rate decreases as the temperature further increases, demonstrating the thermal stability of the resin system. Figure 4(c) presents the non-isothermal DSC curves of the resin system. The curing exothermic peak shifts toward higher temperatures with increasing heating rate β, accompanied by sharper peak shapes, indicating that the heat released from the curing reaction is confined to a narrower temperature range at higher heating rates. The *T*-β extrapolation method was employed to approximate the curing process of the resin system for HMBJ application. As illustrated in Fig. 4(d), linear fittings of the initial curing temperature T_i, peak curing temperature T_p, and final curing temperature T_f at four heating rates combined with extrapolation reveal that at $\beta=0$, T_i, T_p, and T_f of the resin are 138, 249, and 263 ℃, respectively. Consequently, the curing process of the resin system was determined as pre-curing at 138 ℃ for several hours, followed by limited curing at 249 ℃, and post-curing at 263 ℃.

Figure 4(e) shows that at 130, 150, and 180 ℃, the resin required at least 180, 170, and 150 min to complete curing, respectively. The prolonged curing time at medium-to-high temperatures is necessary for the epoxy system to achieve its targeted high-temperature resistance, owing to the intrinsically low reactivity of the heat-resistant resin components.

As shown in Fig. 4(f), the viscosity of the resin decreases gradually with increasing temperature, reaching a minimum value (~10^2 Pa · s) around 130 ℃. A heating rate of 2 ℃/min ensures that the resin flows sufficiently and wets the fibers before the viscosity increases sharply due to the curing reaction. When the temperature reaches near 200 ℃, the complex viscosity rises sharply, indicating rapid resin curing. As shown in Fig. 4(g), the storage modulus and loss modulus curves of the resin system intersect at 125 ℃, marking the gelation temperature, and signifying the onset of crosslinking at 125 ℃. Figure 4(h) reveals that higher temperatures accelerate the rise in resin viscosity. Lower viscosity improves resin fluidity, facilitating full fiber infiltration under pressure. At 130 ℃, the resin maintains a low-viscosity state for approximately 20 min, providing a critical processing window for fiber layer infiltration. The combination of a heating rate of 2 ℃/min and a stepwise curing process from 130 to 180 ℃ optimizes

both the resin flow and the interface bonding quality. The final optimized curing process for the epoxy resin system was established as 130 ℃ (1 h) →150 ℃ (1 h) → 180 ℃ (3 h).

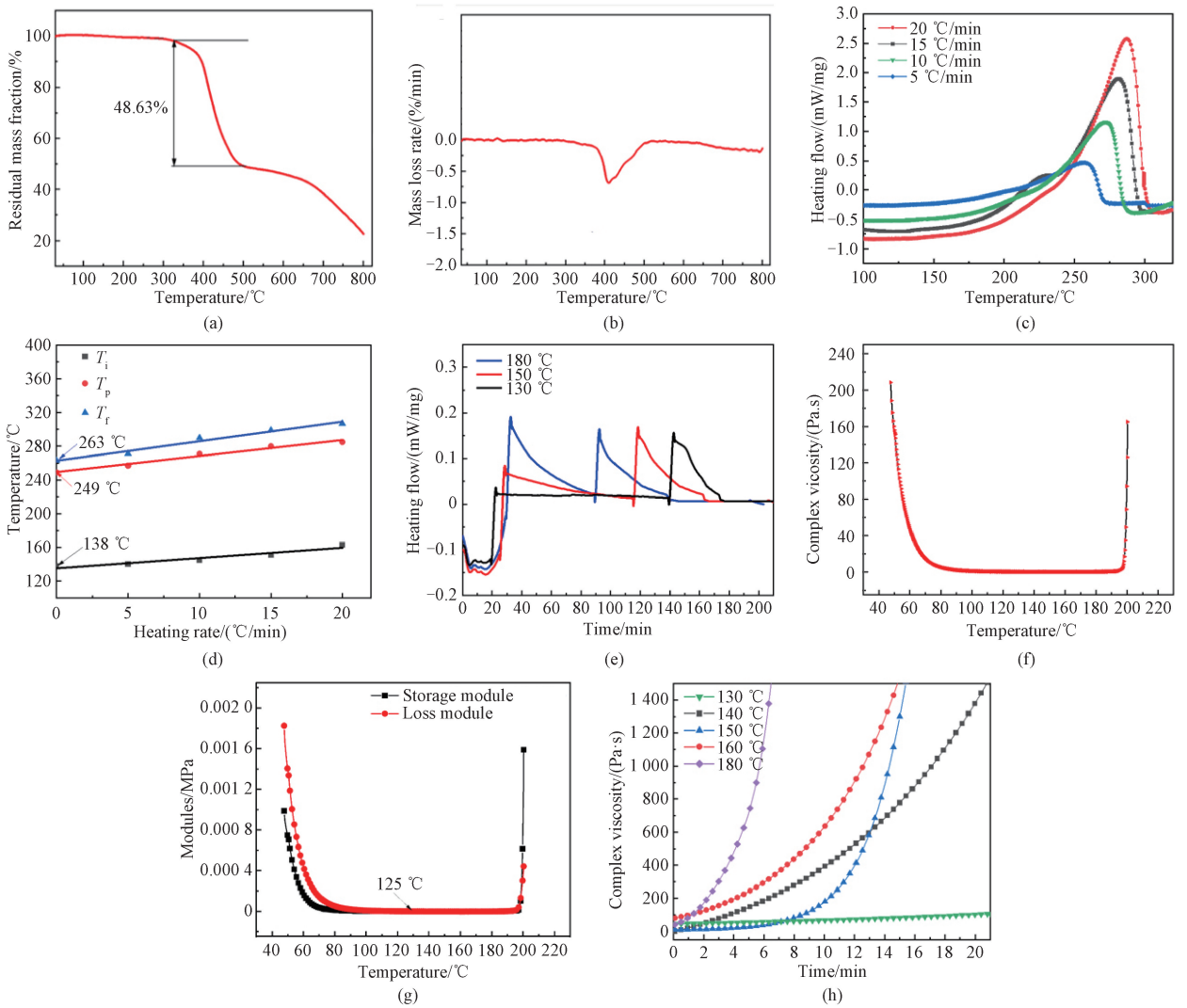


Fig. 4 Thermal and rheological behavior of resin system under different curing conditions: (a) thermogravimetry curve; (b) differential thermogravimetry curve; (c) non-isothermal DSC curves at different heating rates; (d) fitting curves of characteristic temperature with heating rate; (e) isothermal DSC curves at different temperatures; (f) complex viscosity-temperature curve; (g) storage modulus and loss modulus-temperature curves; (h) complex viscosity-time curves at different temperatures

The parameters of different curing processes of CFRP laminates are shown in Fig. 5(a). The low-temperature curing process was set as 115 ℃ (1 h) → 130 ℃ (1 h) →150 ℃ (5 h). In this process, the composite material underwent a prolonged period in the low-temperature gel stage, which increased the resin's viscosity. The resulting greater steric hindrance between polymer molecules prevented the remaining functional groups from fully reacting with the fibers, thereby compromising the interfacial bond strength.

The medium-temperature curing process was set as 130 ℃ (1 h) →150 ℃ (1 h) →180 ℃ (3 h). During this process, the resin maintained a low-viscosity state with optimal fluidity, aiding the gel process. By increasing the temperature, the gel time was reduced, and entering the post-curing stage helped reduce internal resin defects. This allowed the functional groups to react fully, ensuring a tight bond at the resin/fiber interface.

The high-temperature curing process was set as 150 ℃ (1 h) →180 ℃ (1 h) →200 ℃ (1 h). In this process, the resin rapidly solidified at high temperatures, and the gel time was further reduced. This process improved molding efficiency but resulted in considerable thermal stress within the resin matrix, leading to the formation of microcracks.

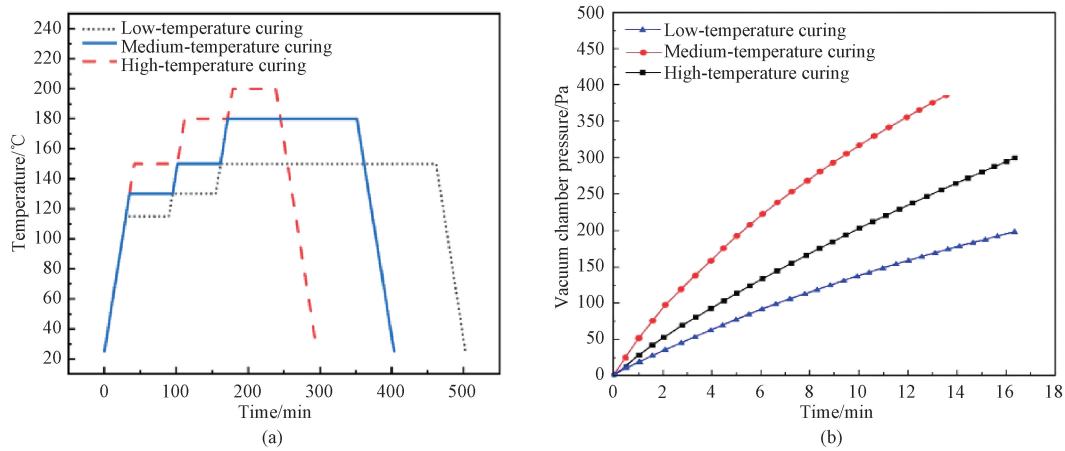


Fig. 5 Gas permeability of CFRP laminates at different curing processes: (a) schematic diagram of different curing processes; (b) gas permeability curves

The oxygen leakage rate of the CFRP laminate cured at low temperature increased by approximately 42.47% compared to that cured at medium temperature (Fig. 5(b) and Table 3). This increase is attributed to the fact that the CFRP resin matrix provides more free-volume holes under low-temperature curing. Additionally, unreacted low-molecular-mass substances are likely to volatilize during use. Unlike the robust three-dimensional network structure of fully cured resin, the undercured parts exhibit a lower crosslinking density and thus impose fewer constraints on molecular chain mobility. This condition creates more pathways for oxygen leakage, leading to increased gas permeability and reduced gas-barrier performance of the laminate.

For CFRP laminates cured at high temperatures, the oxygen leakage rate increased by approximately 84.95%. This is due to the rapid curing process at high temperatures, which hinders the discharge of volatiles within the resin, thereby creating more pores, defects, and microcracks. Despite the more complete curing at high temperatures, this results in an increased leakage rate. Therefore, the curing system needs to be meticulously managed during the molding process of the composite material. This is crucial to ensure the stability of the bond between the resin matrix and the reinforcing fiber and to prevent the formation of internal pores, microdebonding at the fiber/resin interface, and microcracks.

Table 3 Gas-barrier performance of CFRP laminates subjected to different curing processes

Sample	Curing process	Oxygen transmission rate/ [$cm^3/(m^2 \cdot 24\ h \cdot Pa)$]	Oxygen permeability coefficient / [$cm^3 \cdot cm/(cm^2 \cdot s \cdot Pa)$]	Oxygen leakage rate/ ($Pa \cdot m^3/s$)	Oxygen leakage rate deviation/ ($Pa \cdot m^3/s$)
S4	Low-temperature curing	4.36×10^{-5}	6.14×10^{-15}	2.65×10^{-8}	0.11×10^{-8}
S2	Medium-temperature curing	3.06×10^{-5}	4.24×10^{-15}	1.86×10^{-8}	0.08×10^{-8}
S5	High-temperature curing	5.67×10^{-5}	8.07×10^{-15}	3.44×10^{-8}	0.10×10^{-8}

2.3 Effect of overlap mode on gas-barrier performance

For the large-diameter thin-walled cylindrical CFRP HMBJ, cutting the prepreg and overlapping the plies are necessary during the lay-up process. Therefore, based on the previously explored process scheme of six-ply medium-temperature curing with low surface roughness, the influence of different overlap modes on the gas-barrier performance of laminates was studied.

Three overlap modes (termed Overlap 1, Overlap 2, and Overlap 3) were designed. The discontinued plies and overlap joint positions are illustrated in Fig. 6. The gas permeability curves of CFRP laminates with different overlap modes are presented in Fig. 7, and the corresponding data are given in Table 4.

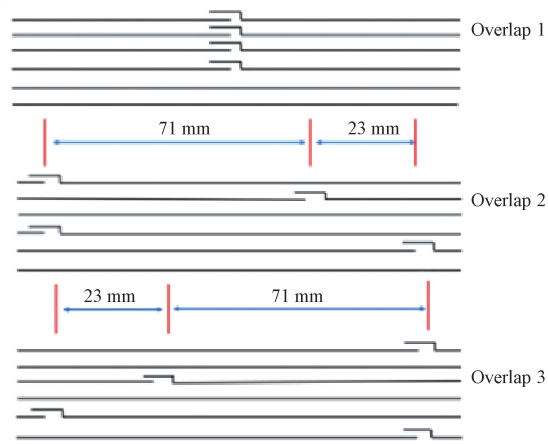


Fig. 6 Distribution of lap joint positions in different overlap modes

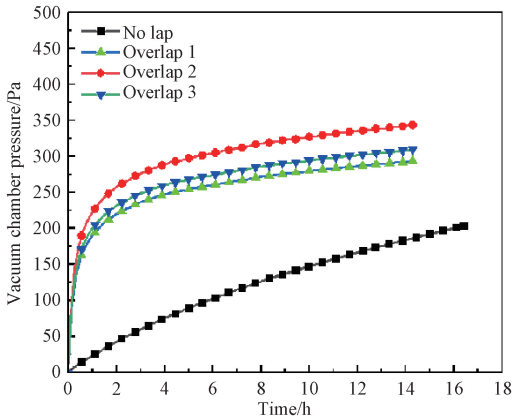


Fig. 7 Gas permeability curves of CFRP laminates with different overlap modes

According to the analysis of Fig. 7 and Table 4, the overlap mode has a specific impact on the gas-barrier performance of CFRP laminates. Compared with no lap bonding, the oxygen leakage rate of CFRP laminates in Overlap 1 increased by 128.17%. This is due to the existence of small gaps or defects at the overlap joint, leading to gas leakage. Simultaneously, each overlap joint is stressed unevenly during the forming process, resulting in increased porosity and defects and decreased gas-barrier performance. Therefore, in the actual lay-up process of the CFRP HMBJ, the ply overlap positions should be maintained uniformly across the lay-up, as excessive non-uniformity can lead to localized gap formation and compromise the gas-barrier performance of the CFRP HMBJ.

Table 4 Gas-barrier performance of CFRP laminates with different overlap modes

Sample	Overlap mode	Oxygen transmission rate/ [$cm^3/(m^2 \cdot 24\ h \cdot Pa)$]	Oxygen permeability coefficient/ [$cm^3 \cdot cm/(cm^2 \cdot s \cdot Pa)$]	Oxygen leakage rate/ ($Pa \cdot m^3/s$)	Oxygen leakage rate deviation/ ($Pa \cdot m^3/s$)
S6	No lap	2.34×10^{-5}	3.34×10^{-15}	1.42×10^{-8}	0.09×10^{-8}
S7	Overlap 1	5.34×10^{-5}	7.65×10^{-15}	3.24×10^{-8}	0.50×10^{-8}
S8	Overlap 2	5.79×10^{-5}	8.16×10^{-15}	3.52×10^{-8}	0.68×10^{-8}
S9	Overlap 3	6.26×10^{-5}	8.86×10^{-15}	3.80×10^{-8}	0.75×10^{-8}

2.4 Gas-barrier performance analysis of CFRP laminates

Figure 8 shows the fiber/resin distribution in the cross-section of the CFRP laminates. The cross-sectional view after curing demonstrates minimal resin-rich areas or dry spots, indicating an effective pressure balance during the molding process. It can be found that there is a slight debonding phenomenon between the fiber/resin interfaces. Similarly, no microcrack is located across the entire section of the CFRP laminates. The test results of the oxygen leakage rate of the CFRP laminates show that the oxygen leakage rate of all the laminates is of the same order of magnitude, indicating that there is no microcrack through the entire section[26], which would otherwise significantly degrade the gas-barrier performance. In the absence of severe internal defects, gas molecules diffuse through CFRP laminates according to the diffusion-leakage theory for composite materials. However, a slightly debonded interface between the carbon fiber and epoxy resin can provide a preferential path for oxygen molecules, leading to increased leakage along this interface. According to the theoretical analysis by Hamori et al.[30], the primary reason for the failure of composite laminates is the formation of gas leakage paths through interlayer microcracks penetrating the composite interior. Consequently, the gas-barrier performance of the composite could be enhanced by optimizing the lay-up design and elongating the gas leakage path.

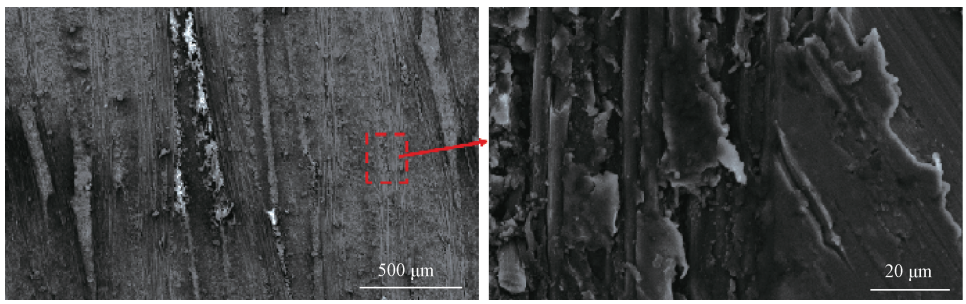
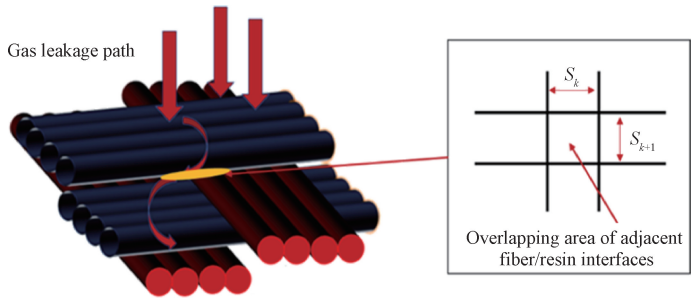


Fig. 8 Cross-sectional SEM image of fiber/resin distribution in CFRP: (a) CFRP laminate cross-section; (b) microdebonding area at the fiber/resin interface

The gas permeability caused by microcrack penetration in composite laminates is a function related to crack opening displacement. Based on the gas leakage path along the fiber/resin microdebonding interface in composite laminates, we applied the microcrack leakage model established by Kumazawa et al.[31]. It is assumed

that the oxygen transmission rate of the composite laminates is a function of the interface microdebonding displacement, and the gas leakage path in the CFRP laminates is illustrated in Fig. 9.



S_k— the debonding displacement of the fiber/resin interface in the kth ply of composite laminates.

Fig. 9 Schematic diagram of oxygen leakage in overlapping area of adjacent fiber/resin interfaces

Based on the leakage condition of the interface slightly debonding, the oxygen transmission rate can be expressed as[31]

$$Q_g = C \cdot \Delta P, \tag{1}$$

where Q_g is the oxygen transmission rate through the laminate; C is the oxygen leakage conductivity; ΔP is the pressure difference between the two sides of the composite laminate.

The oxygen leakage conductivity C is related to the leakage conductivity C_k of each ply.

$$C_k = f \cdot S_k \cdot S_{k+1}, \tag{2}$$

where C_k is the oxygen leakage conductivity of the kth ply in composite laminates; f is the oxygen permeability coefficient.

The relationship between C and C_k is

$$C = \left(\sum_{k=1}^{n} \frac{1}{C_k} \right)^{-1}, \tag{3}$$

where n is the total number of plies. Consequently, the relationship between Q_g and S_k is

$$Q_g = \left(\sum_{k=1}^{n} \frac{1}{f \cdot S_k \cdot S_{k+1}} \right)^{-1} \cdot \Delta P. \tag{4}$$

Equation (4) indicates that the smaller the value of microdebonding displacement at the interface between the fiber and resin in the composite laminate, the better the gas-barrier performance of the composite laminate. An effective way to improve the gas-barrier performance of composite laminates is to strengthen the fiber/resin interfacial bonding and minimize the occurrence of microdebonding.

2.5 Gas leakage performance analysis of HMBJ

The helium injection method and vacuum method were combined to test the overall helium leakage rate of the CFRP HMBJ. To ensure that the CFRP HMBJ can provide a stable internal environment and maintain the stable operation of the internal hydrogen beam under the simulated space conditions, the helium leakage rate of the CFRP HMBJ under the experimental conditions was required to be lower than 1×10^{-6} Pa · m^3/s.

During the actual test, when the helium leak detector was used to measure the leakage rate, it was necessary to account for the background helium content within the helium leak detector itself. After sealing the HMBJ with a sealed bag and injecting a suitable amount of helium, the helium leakage rate curve stabilized for a certain period. The detected helium leakage rate of the CFRP HMBJ was 9.04×10^{-7} Pa · m^3/s, lower than the specified limit of 1×10^{-6} Pa·m^3/s.

3 Conclusions

To improve the gas-barrier performance of CFRP laminates, CFRP laminates with different ply counts, curing processes, and overlap modes were prepared using the die-pressing process. According to the GB/T 1038.1—2020 pressure difference method, the gas-barrier performance of the CFRP laminates was tested, and the influence rules were analyzed. The key findings of this study are as follows.

1) With an increase in the ply counts, the oxygen leakage rate of CFRP laminates decreased, leading to an enhancement in gas-barrier performance. To fulfill the goal of reducing mass by 30% while maintaining the sealing performance of the HMBJs, six plies were selected for the CFRP laminates after calculating the ideal HMBJ mass. Compared with medium-temperature curing, the oxygen leakage rates of CFRP laminates cured at low and high temperatures increased by 42.47% and 84.95%, respectively. The oxygen leakage rate for CFRP laminates with interlayer overlap was found to be at least 128.17% higher than that of CFRP laminates without overlap.

2) The decomposition temperature of the CFRP resin system (330 ℃) was significantly higher than the typical operating temperature range of satellite hydrogen masers in space environments (−150 to 150 ℃), ensuring structural integrity under extreme temperature cycles during orbital operations.

3) By increasing the ply count, reducing overlaps, and optimizing the curing process, the gas-barrier performance of CFRP laminates was effectively improved. The CFRP HMBJ exhibited a helium leakage rate of 9.04×10^{-7} Pa·m^3/s, meeting the requirements for gas-barrier performance. The CFRP HMBJ was 34.9% lighter than the AA-7075 HMBJ (830 g). The target of 30% mass reduction was achieved.

In summary, the CFRP HMBJ fabricated in this study satisfies all specified performance criteria. The process design, which takes into account gas-barrier performance, cost-effectiveness, and manufacturability, has been demonstrated to be both stable and feasible.

References

[1] Wang W, Wang Y, Yu C, et al. Spaceborne atomic clock performance review of BDS-3 MEO satellites[J]. *Measurement*, 2021, 175: 109075.

[2] Zhu Y, Zhang Q, Mao Y, et al. Comprehensive performance review of BDS-3 after one-year official operation [J]. *Advances in Space Research*, 2023, 71(1): 883-899.

[3] Priyanka S, Gu B H. Effect of thermo-oxidative aging on flexural behavior of quasi-isotropic carbon fiber reinforced composite laminates[J]. *Journal of Donghua University (English Edition)*, 2025, 42(3): 259-272.

[4] Wan Y, Straumit I, Takahashi J, et al. Micro-CT analysis of internal geometry of chopped carbon fiber tapes reinforced thermoplastics[J]. *Composites Part A: Applied Science and Manufacturing*, 2016, 91: 211-221.

[5] Behzad T, Sain M. Finite element modeling of polymer curing in natural fiber reinforced composites [J]. *Composites Science and Technology*, 2007, 67(7/8): 1666-1673.

[6] Ozaki H, Nakada M, Uzawa K, et al. Effect of molding condition on flexural strength of textile carbon fiber reinforced polycarbonate laminates [J]. *Journal of Reinforced Plastics and Composites*, 2014, 33(20): 1893-1901.

[7] Mann G S, Singh L P, Kumar P, et al. Effect of process parameters on the fabrication of hybrid natural fiber composites fabricated via compression moulding process[J]. *Journal of Natural Fibers*, 2022, 19(16): 14803-14812.

[8] Liu J, Wang X F, Chang X P. Numerical simulation on cracked plate repaired with carbon-fiber wrapped composite material[J]. *Advanced Materials Research*, 2012, 512: 1664-1667.

[9] Ding A, Li S, Wang J, et al. Prediction of process-induced distortions in L-shaped composite profiles using path-dependent constitutive law [J]. *Applied Composite Materials*, 2016, 23(5): 1027-1045.

[10] Nyflött Å, Petkova-Olsson Y, Moons E, et al. Modeling of oxygen permeation through filled polymeric layers for barrier coatings[J]. *Journal of Applied Polymer Science*, 2017, 134(20): 44834.

[11] Barton J M, Buist G J, Deazle A S, et al. The application of molecular simulation to the rational design of new materials: 1. Structure and modelling studies of linear epoxy systems[J]. *Polymer*, 1994, 35(20): 4326-4333.

[12] Abderrezak B, Mehdi M, Drouiche N, et al. Progress of fitting models describing transport phenomena within nanofiltration membranes: a review[J]. *Desalination and Water Treatment*, 2020, 184: 94-129.

[13] Kucukpinar E, Doruker P. Molecular simulations of small gas diffusion and solubility in copolymers of styrene[J]. *Polymer*, 2003, 44(12): 3607-3620.

[14] He Y, Chen Q, Yang S, et al. Micro-crack behavior of carbon fiber reinforced Fe_3O_4/graphene oxide modified epoxy composites for cryogenic application[J]. *Composites Part A: Applied Science and Manufacturing*, 2018, 108: 12-22.

[15] Yokozeki T, Aoki T, Ishikawa T. Experimental cryogenic gas leakage through damaged composite laminates for propellant tank application [J]. *Journal of Spacecraft and Rockets*, 2005, 42(2): 363-366.

[16] Choi S, Sankar B V. Micromechanical analysis of composite laminates at cryogenic temperatures [J]. *Journal of Composite Materials*, 2006, 40(12): 1077-1091.

[17] Choi S, Sankar B V. Gas permeability of various graphite/epoxy composite laminates for cryogenic storage systems [J]. *Composites Part B: Engineering*, 2008, 39(5): 782-791.

[18] Yokozeki T, Ogasawara T, Aoki T, et al. Experimental evaluation of gas permeability through damaged composite laminates for cryogenic tank [J]. *Composites Science and Technology*, 2009, 69(9): 1334-1340.

[19] Bois C, Malenfant J C, Wahl J C, et al. A multiscale damage and crack opening model for the prediction of flow path in laminated composite [J]. *Composites Science and Technology*, 2014, 97: 81-89.

[20] Yokozeki T, Aoki T, Ishikawa T. The effect of matrix cracks on gas permeability through CFRP laminates[J]. *Advanced Composite Materials*, 2004, 13(3/4): 227-236.

[21] Hamori H, Kumazawa H, Higuchi R, et al. Numerical and experimental evaluation of the formation of leakage paths through CFRP cross-ply laminates with leak barrier layers [J]. *Composite Structures*, 2019, 230: 111530.

[22] Katsivalis I, Signorini V, Ohlsson F, et al.

Hydrogen permeability of thin-ply composites after mechanical loading[J]. *Composites Part A: Applied Science and Manufacturing*, 2024, 176: 107867.
[23] Kumazawa H, Susuki I, Aoki T. Gas leakage evaluation of CFRP cross-ply laminates under biaxial loadings [J]. *Journal of Composite Materials*, 2006, 40(10): 853-871.
[24] Kumazawa H, Aoki T, Susuki I. Influence of stacking sequence on leakage characteristics through CFRP composite laminates [J]. *Composites Science and Technology*, 2006, 66(13): 2107-2115.
[25] Kumazawa H, Whitcomb J. Numerical modeling of gas leakage through damaged composite laminates[J]. *Journal of Composite Materials*, 2008, 42(16): 1619-1638.
[26] Meng J, Zheng H, Wei Y, et al. Leakage performance of CFRP laminate under cryogenic temperature: experimental and simulation study [J]. *Composites Science and Technology*, 2022, 226: 109550.
[27] Yokozeki T, Aoki T, Ogasawara T, et al. Effects of layup angle and ply thickness on matrix crack interaction in contiguous plies of composite laminates [J]. *Composites Part A: Applied Science and Manufacturing*, 2005, 36(9): 1229-1235.
[28] Wei R, Wang X, Chen C, et al. Effect of surface treatment on the interfacial adhesion performance of aluminum foil/CFRP laminates for cryogenic propellant tanks[J]. *Materials & Design*, 2017, 116: 188-198.
[29] Lin N. Measurement and analysis of permeability of large tow carbon fiber warp knitted fabric[J]. *Petrochemical Technology and Economics*, 2024, 40(3): 24-27. (in Chinese)
[30] Hamori H, Kumazawa H, Higuchi R, et al. Gas permeability of CFRP cross-ply laminates with thin-ply barrier layers under cryogenic and biaxial loading conditions [J]. *Composite Structures*, 2020, 245: 112326.
[31] Kumazawa H, Aoki T, Susuki I. Analysis and experiment of gas leakage through composite laminates for propellant tanks[J]. *AIAA Journal*, 2003, 41(10): 2037-2044.

气体阻隔性能优异的 CFRP 氢钟钟罩

高建东[1,2]，肖　德[1,2]，程乐乐[1,2]，陈志钢[1,2]，帅　涛[3*]，张丽莎[4*]，余木火[1,2]，孙泽玉[1,2*]

1. 东华大学 先进纤维材料全国重点实验室，材料科学与工程学院，上海 201620
2. 东华大学 上海轻质结构复合材料重点实验室，上海高性能纤维与复合材料协同创新中心，上海 201620
3. 中国科学院上海天文台，上海 200030
4. 东华大学 环境科学与工程学院，上海 201620

摘　要：研究了用于氢钟钟罩的碳纤维增强聚合物（carbon fiber reinforced polymer，CFRP）层压板的气体阻隔优化问题。通过系统分析铺层的层数、固化工艺及层间搭接方式等关键因素对 CFRP 层压板气体阻隔性能的影响，采用 CATIA 软件进行设计，通过模压工艺，成功制备出具有优异气体阻隔性能的 CFRP 氢钟钟罩。与铝合金氢钟钟罩相比，CFRP 模压成型氢钟钟罩质量减轻 34.9%，氦气泄漏率低至 9.04×10^{-7} Pa·m^3/s，满足氢钟罩性能要求。研究表明，CFRP 层压板中气体主要通过纤维/树脂界面扩散泄漏，这为模压成型 CFRP 氢钟钟罩同时实现密封性与结构优化提供了理论依据。CFRP 模压钟罩兼具成本低、工艺简单及抗泄漏性能优等优势，为卫星氢钟钟罩提供了一种合理的解决方案。

关键词：碳纤维增强聚合物；模压工艺；气体阻隔性能；树脂固化体系；层间搭接